COSMOLOGICAL CONSTRAINTS FROM THE ROSAT DEEP CLUSTER SURVEY

Stefano Borgani[1], Piero Rosati[2], Paolo Tozzi[3,4] & Colin Norman[4]

[1] INFN, Sezione di Perugia, c/o Dipartimento di Fisica dell'Università, via A. Pascoli, I-06123 Perugia (Italy)
E-mail: stefano.borgani@perugia.infn.it

[2] ESO – European Southern Observatory, D-85748 Garching bei München (Germany)
E-mail: prosati@eso.org

[3] Dipartimento di Fisica, II Università di Roma, via Ricerca Scientifica 1, I-00133 Roma (Italy)

[4] Department of Physics and Astronomy, The Johns Hopkins University, Baltimore, MD 21218 (U.S.A.)
E-mail: tozzi, norman@stsci.edu

arXiv:astro-ph/9901017v1 4 Jan 1999

ABSTRACT

The ROSAT Deep Cluster Survey (RDCS) has provided a new large deep sample of X–ray selected galaxy clusters. Observables such as the flux number counts $n(S)$, the redshift distribution $n(z)$ and the X-ray luminosity function (XLF) over a large redshift baseline ($z \lesssim 0.8$) are used here in order to constrain cosmological models. Our analysis is based on the Press–Schechter approach, whose reliability is tested against N–body simulations. Following a phenomenological approach, no assumption is made *a priori* on the relation between cluster masses and observed X–ray luminosities. As a first step, we use the local XLF from RDCS, along with the high–luminosity extension provided by the XLF from the Brightest Cluster Survey, in order to constrain the amplitude of the power spectrum, σ_8, and the shape of the local luminosity–temperature, L_{bol}–T, relation. We obtain $\sigma_8 = (0.58 \pm 0.06) \times \Omega_0^{-0.47+0.16\Omega_0}$ for flat models ($\Omega_\Lambda = 1 - \Omega_0$) and $\sigma_8 = (0.58 \pm 0.06) \times \Omega_0^{-0.53+0.27\Omega_0}$ for open models ($\Omega_\Lambda = 0$) at 90% confidence level, almost independent of the L_{bol}–T shape. The density parameter Ω_0 and the evolution of the L_{bol}–T relation are constrained by the RDCS XLF at $z > 0$ and the EMSS XLF at $\bar{z} = 0.33$, and by the RDCS $n(S)$ and $n(z)$ distributions. By modelling the evolution for the amplitude of the L_{bol}–T relation as $(1+z)^A$, an $\Omega_0 = 1$ model can be accommodated for the evolution of the XLF with $1 \lesssim A \lesssim 3$ at 90% confidence level, while $\Omega_0 = 0.4^{+0.3}_{-0.2}$ and $\Omega_0 \lesssim 0.6$ are implied by a non–evolving L_{bol}–T ($A = 0$) for open and flat models, respectively.

Subject headings: Cosmology: theory - dark matter - galaxies: clusters: general - X-rays: galaxies

1 Introduction

Galaxy clusters are crucial probes for models describing the formation and evolution of cosmic structures. In standard scenarios, clusters form at high peaks of the primordial density field (e.g., Kaiser 1984; Bardeen et al. 1986). Therefore, both the statistics of their large–scale distribution and their abundance are highly sensitive to the nature of the underlying dark matter density field. Furthermore, their typical scale, $\sim 10\,h^{-1}$Mpc (h is the Hubble constant in units of $100\,\mathrm{km\,s^{-1}}Mpc^{-1}$), relates to fluctuation modes which have still to enter, or are just approaching, the non–linear stage of gravitational evolution. Then, although their internal gravitational and gas dynamics are rather complex, a statistical description of global cluster properties can be provided by resorting to linear theory or perturbative approaches. By following the redshift evolution of clusters, we have a valuable method to trace the global dynamics of the Universe and, therefore, to determine its geometry.

In this context, the cluster abundance at a given mass has long been recognized as a stringent test for cosmological models. Typical rich clusters have masses of about $5 \times 10^{14} h^{-1} M_\odot$, which is quite similar to the average mass within a sphere of $\sim 8\,h^{-1}$Mpc radius in the unperturbed universe. Therefore, the local abundance of clusters is expected to place a constraint on σ_8, the r.m.s. fluctuation on the $8\,h^{-1}$Mpc scale. Analytical arguments based on the approach devised by Press & Schechter (1974) show that the cluster abundance is highly sensitive to σ_8 for a given value of the density parameter Ω_0 (e.g., Frenk et al. 1990; Bahcall & Cen 1992; Lilje 1992; White, Efstathiou & Frenk 1993; Viana & Liddle 1996). Once a model is tuned so as to predict the correct abundance of local ($z \lesssim 0.1$) clusters, its evolution will mainly depend on Ω_0 (e.g., Oukbir & Blanchard 1992). Hence, the possibility of tracing the evolution of the cluster abundance with redshift should provide both the value of the density parameter and the amplitude of the fluctuations at the cluster scale.

It is worth stressing, however, that by 'abundance' one means the comoving volume density of galaxy clusters *per unit mass*, which cannot be directly observed. Therefore, these arguments always assume a relation of some observable cluster property to the total mass. In this respect, X-ray selected samples have been proved to be extremely useful, essentially due to the simplicity of their selection functions.

The availability of new observational data for high–z clusters has recently stimulated a flurry of activity in this direction. For instance, Carlberg et al. (1997) and Fan, Bahcall & Cen (1997) have used results on the internal velocity dispersion σ_v of X-ray selected clusters in the CNOC survey (Carlberg et al. 1996) and concluded that low–density models with $\sigma_8 \simeq 0.7$–0.9 and $\Omega_0 \simeq 0.3$–0.5 are preferred (see, however, Gross et al. 1998).

Observations of cluster X-ray temperatures offer an independent and powerful means to characterize the evolution of the cluster abundance since cluster temperatures are directly connected to cluster masses. Eke, Cole & Frenk (1996) have pointed out that a measurement of the cluster temperature distribution at $z \simeq 0.5$ would discriminate at a high confidence level between a critical density model and a low–density model with $\Omega_0 \simeq 0.3$. First attempts in this direction have been pursued by Henry (1998) and Eke et al. (1998) who used available data on the X–ray temperature function for $z \lesssim 0.4$ and found $\sigma_8 \simeq 0.5$–0.8 and $\Omega_0 \simeq 0.3$–0.7. Based on a similar data set, a different conclusion has been however reached by Viana & Liddle (1998), who argued that a critical–density Universe is still viable as far as the evolution of the cluster temperature function is concerned. More robust results will require substantially larger compilations of cluster temperatures, which will be a time consuming process even with the next generation of X-ray satellites.

An alternative way to trace the evolution of the cluster abundance is to rely on the luminosity distribution of X-ray flux–limited cluster samples (e.g., Henry et al. 1992; Oukbir & Blanchard 1992; Bartlett & Silk 1993; Colafrancesco & Vittorio 1994; Reichart et al. 1998). The advantage of this approach lies in the simplicity of the measurement and the availability of large samples, with well understood selection biases. A good understanding of hydrodynamical processes in the intra–cluster medium (ICM), as well as feedback mechanisms from stellar energy release, are however needed in order to relate the X–ray luminosity to the cluster mass.

Following the original samples from the Einstein Medium Sensitivity Survey (EMSS; Gioia et al. 1990), the ROSAT-PSPC has recently given a strong impulse in this area providing both large solid angle, high flux limit samples (e.g. the Bright Cluster Sample (BCS) by Ebeling et al. 1997), and more distant cluster samples from deeper, small solid angle surveys (the ROSAT Deep Cluster Survey (RDCS) by Rosati et al. 1995, 1998; WARPS by Scharf et al. 1997; SHARC-S by Burke et al. 1997 and Collins et al. 1997; the sample based on ROSAT PSPC by Vikhlinin et al. 1998).

In this paper, we use, for the first time, the complete amount of information contained in the RDCS, namely the evolving X–ray luminosity function (XLF), the deepest flux number counts and the redshift distribution, along with a knowledge of the RDCS selection function. In particular, in order to normalize the models at $z \sim 0$ we will use the local XLF from the RDCS and the high–luminosity extension from BCS. Then, we will use the XLF estimates from RDCS at the median redshifts $\bar{z} \simeq 0.3$ and $\bar{z} \simeq 0.6$, the flux–number counts $n(S)$ and the redshift distribution $n(z)$ from the RDCS to constrain the evolution. We note that the number counts and redshift distribution represent the projection of the z–dependent XLF along the redshift and flux, respectively. The number counts alone from the RDCS have been already used by different authors to place constraints on cosmological models (see Kitayama & Suto 1997; Mathiesen & Evrard 1998 for a parametric approach; see Cavaliere, Menci & Tozzi 1998 for an approach based on a physical models for the ICM).

Instead of relying on specific physical models to describe the ICM and its evolution, we prefer here to adopt a phenomenological approach. Using a parameteric expression for the relation between cluster masses and X–ray luminosities, we fit the corresponding parameters, along with those describing the cosmological models, to match the RDCS data.

The two principal issues addressed in this paper are to: (1) derive robust constraints on the amplitude of fluctuations on the cluster mass scale using the local XLF and; (2) derive robust constraints on Ω_0 and the L_{bol}–T relation from a flux–limited sample of clusters with $z \lesssim 1$, like RDCS.

The structure of the paper is as follows. In Section 2 we give a brief description of the data, while in Section 3 we present the method of analysis. We review the Press–Schechter approach for the mass function and compare its predictions with a set of P3M N–body simulations in order to assess its reliability. Then, we describe in detail our procedure to convert cluster masses into luminosities. This will be accomplished in three steps: *(i)* converting virial masses into temperatures; *(ii)* converting temperatures into bolometric luminosities; *(iii)* correcting luminosities from the bolometric to the soft *ROSAT* [0.5-2.0] keV band. In Section 4 we present the results of this analysis from the local XLF to constrain the shape and the amplitude σ_8 of *COBE*–normalized power–spectra as well as the local luminosity–temperature (L_{bol}–T) relation. In Section 5 we use the evolving XLF, number counts and redshift distribution to constrain the density parameter Ω_0 and the evolution of L_{bol}–T. A brief discussion of the results and the main conclusions are given in Section 6.

2 The RDCS sample

The RDCS compiled a large, X-ray flux limited sample of galaxy clusters, selected on the basis of X-ray properties alone, via a serendipitous search in ROSAT-PSPC deep pointed observations (Rosati et al. 1995). The depth and solid angle of the survey were chosen to probe an adequate range of X-ray luminosities over a large redshift baseline. Over 160 cluster candidates were selected down to the flux limit of $S = 1 \times 10^{-14}\,\mathrm{erg\,s^{-1}cm^{-2}}$, over an area of 50 deg^2, by utilizing a wavelet-based detection technique. The latter is particularly efficient in discriminating between point-like and extended, low surface brightness sources. The completeness and degree of contamination of the catalogue are well understood above $S = 2 \times 10^{-14}\,\mathrm{erg\,s^{-1}cm^{-2}}$, but still uncertain at lower fluxes where the optical identification program is not yet complete. The sky coverage of the survey, a crucial ingredient in the interpretation of deep cluster surveys, has also been extensively studied (Rosati et al. 1998; RDNG hereafter). Cluster redshifts have been secured for more than 100 clusters/groups to date using NOAO and ESO

telescopes. In this paper, we use the flux limited subsample of spectroscopically identified clusters used by RDNG to derive the cluster XLF. This comprises 70 clusters with fluxes $S \geq 4 \times 10^{-14}\,\mathrm{erg\,s^{-1}cm^{-2}}$ and $0.05 \lesssim z \lesssim 0.85$. The whole RDCS sample is used to compare model predictions with the observed cluster number counts. An additional determination is included in the present analysis at the faintest bin ($S < 2 \times 10^{-14}\,\mathrm{erg\,s^{-1}cm^{-2}}$) which extends the Log N–Log S presented by RDNG. We note that 15% of the cluster candidates, mostly at the faint end, still remain to be optically identified.

3 The Theoretical framework

3.1 The recipe for the cluster mass function

3.1.1 The power spectrum model

We write the linear power spectrum of density fluctuations as $P(k) \propto k^{n_{pr}} T^2(k)$. For the transfer function $T(k)$, we assume the Gamma–model

$$T(q) \,=\, \frac{\ln(1+2.34q)}{2.34q} \times \left[1+3.89q+(16.1q)^2+(5.46q)^3+(6.71q)^4\right]^{-1/4} \quad (1)$$

where $q = k/h\Gamma$, being Γ the shape parameter. For the class of CDM models, it is $\Gamma \simeq \Omega_0 h$ (Bardeen et al. 1986), while in general Γ can be viewed as a free parameter, to be fitted to observational constraints. For instance, for the $\Omega_0 = 1$, case $\Gamma \simeq 0.2$ can be obtained either in the framework of Cold+Hot DM models with a suitable choice of the massive neutrino fraction (e.g., Primack 1997), or in the framework of τCDM models, where the CDM shape of $P(k)$ is modified by the decay of massive neutrinos (White, Gelmini & Silk 1995). As for the primordial spectral index, n_{pr}, we will mainly concentrate in the following on the Harrison–Zeldovich case $n_{pr} = 1$, although we will also comment about the effect of varying n_{pr} around this value. As usual, the amplitude of $P(k)$ will be expressed in terms of σ_8 and is fixed by the four–year *COBE* normalization recipe, as provided by Bunn & White (1997) and Hu & White (1997) for the $\Omega_\Lambda = 1 - \Omega_0$ and the $\Omega_\Lambda = 0$ cases, respectively. This normalization determines a one-to-one correspondence between σ_8 and the shape parameter Γ for a fixed value of n_{pr}.

3.1.2 The Press–Schechter approach

According to the PS formalism, clusters at a given redshift, z, are identified with those halos that are just virializing. The comoving number density of such structures in the mass range $[M, M+dM]$ reads

$$\frac{dn}{dM} \,=\, \sqrt{\frac{2}{\pi}}\,\frac{\bar\rho}{M^2}\,\frac{\delta_c(z)}{\sigma_M}\,\left|\frac{d\log\sigma_M}{d\log M}\right|\,\exp\left(-\frac{\delta_c(z)^2}{2\sigma_M^2}\right)\,. \quad (2)$$

Here $\bar\rho$ is the present day average matter density and $\delta_c(z)$ is the linear–theory overdensity extrapolated at the present time for a uniform spherical fluctuation collapsing at redshift z. This quantity conveys information about the dynamics of fluctuation evolution in a generic Friedmann background. It is convenient to express it as $\delta_c(z) = \delta_0(z)\,[D(0)/D(z)]$, where

$$D(z) \,=\, \frac{5}{2}\,\Omega_0 E(z)\,\int_z^\infty \frac{1+z'}{E(z')^3}\,dz' \quad (3)$$

is the linear fluctuation growth factor. In the above expression, $E(z) = [(1+z)^3\Omega_0 + (1+z)^2\Omega_R + \Omega_\Lambda]^{1/2}$, where $\Omega_\Lambda = \Lambda/3H^2$ and $\Omega_R = 1 - \Omega_0 - \Omega_\Lambda$ (see, e.g., Peebles 1993).

The quantity $\delta_0(z)$ has a weak dependence on Ω_0 for both $\Omega_\Lambda = 0$ and $\Omega_R = 0$. In the following we will adopt for $\delta_0(z)$ the expression provided by Kitayama & Suto (1996). For a critical–density Universe it is $\delta_c(z) = 1.686(1+z)$.

The rms density fluctuation at the mass scale M, σ_M, is connected to the fluctuation power spectrum according to

$$\sigma_M^2 \,=\, \frac{1}{2\pi^2}\,\int_0^\infty dk\,k^2\,P(k)\,W^2(kR)\,. \quad (4)$$

Here $W(x)$ is the Fourier representation of the window function, which describes the shape of the volume from which the collapsing object is accreting matter. The comoving fluctuation size R is connected to the mass scale M as $R = (3M/4\pi\bar\rho)^{1/3}$ for the top–hat window, $W(x) = 3(\sin x - x\cos x)/x^3$, that we adopt in the following.

3.1.3 Comparison with N–body simulations

The reliability of the PS formula has been tested against N–body simulations by several authors. As a general result, it turns out that eq.(2) provides an overall satisfactory description of the N–body mass function around the non–linear mass scale M_* (i.e., the mass at which $\delta_c(z)/\sigma_{M_*} = 1$), which controls the position of the exponential cut–off (e.g., Lacey & Cole 1993; Eke et al. 1996).

In order to make our own comparison, we ran a set of N–body simulations for three different models. Simulations are run for: *(a)* an $\Omega_0 = 1$ model with $n_{pr} = 0.8$ and $\Gamma = 0.35$; *(b)* a flat low–density model with $\Omega_0 = 0.4$ and $\Gamma = 0.22$; *(c)* an open model with $\Omega_0 = 0.6$ and $\Gamma = 0.25$. Model parameters are described in Table 1. They have been chosen in such a way that the corresponding power spectra are consistent with the APM galaxy $P(k)$ shape (e.g., Baugh & Efstathiou 1993), the local cluster number density (e.g., Eke et al. 1996; Girardi et al. 1998) and the CMB anisotropies from the 4–year *COBE* data (e.g., Gorskì et al. 1996).

Each simulation is run within a box of $\mathcal{L} = 250\,h^{-1}$Mpc a side using the adaptive particle-particle–particle-mesh (AP3M) code, kindly provided by Couchman (1991). The code follows the trajectories of 128^3 particles, with a comoving equivalent Plummer softening parameter of $\simeq 100\,h^{-1}$ kpc. Therefore, both the mass resolution ($m_{part} \simeq 2.06 \times 10^{12}\Omega_0\,h^{-1}M_\odot$ for the mass of each particle) and the dynamical resolution are adequate to describe halo masses

down to poor clusters ($\lesssim 10^{14} h^{-1} M_\odot$). The initial redshift z_i at which simulations are started has been fixed so that $\sigma = 0.2$ for the r.m.s. fluctuation amplitude on the grid at that time. The integration variable is chosen to be $p = a^{3/2}$, where $a = (1+z)^{-1}$ is the expansion factor. The number of time–steps has been determined by fixing $\Delta p = 0.14$. This ensured an energy conservation of about 3% at the final step of each simulation. For each model, we run five different realizations in order to have enough statistics to reliably estimate the mass function in the high–mass tail.

TABLE 1

PARAMETERS OF THE SIMULATION MODELS

Model	Ω_0	n_{pr}	Γ	σ_8	z_i	Time–steps
EdS	1.0	0.8	0.35	0.56	10	240
Flat	0.4	1.0	0.22	0.87	16	480
Open	0.6	1.0	0.25	0.67	15	440

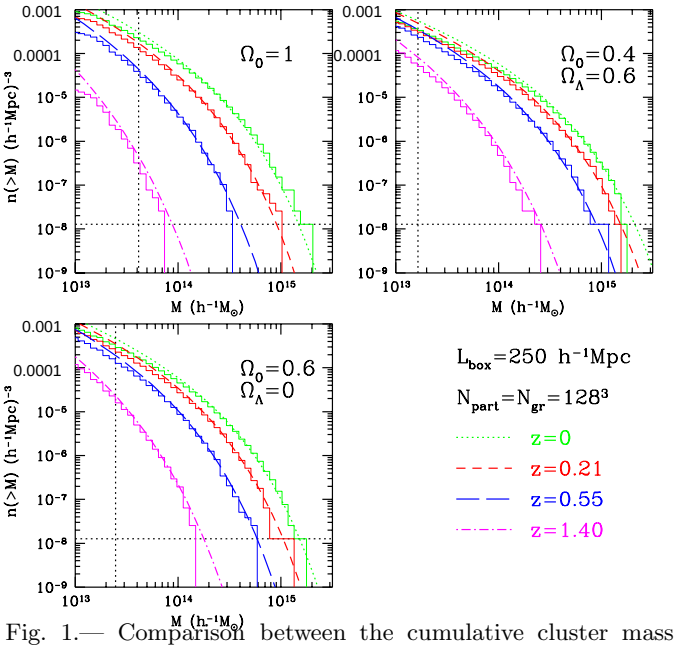

Fig. 1.— Comparison between the cumulative cluster mass function $n(>M)$ produced by N-body simulations (histograms) and the Press–Schechter formula (smooth curves) at different redshifts. Details about the parameters of the simulated models are provided in Table 1. The horizontal dotted line indicates the shot-noise level, i.e. the cluster number density associated with one single cluster in the volume of the five simulation boxes. The vertical dotted lines indicates the minimum fiducial mass for a cluster to be reliably identified, i.e. corresponding to a cluster resolved with 20 particles.

Clusters in each simulation are identified by following a two–step procedure. Firstly, we apply a friend-of-friends (FOF) algorithm with linking parameter $b = 0.2$ in order to identify cluster candidates. For each FOF group, we compute the center of mass of the particles that belong to it. Therefore, starting from each center, draw a sphere whose radius encompasses an average density equal to the virial density: $\rho_{vir}(z) = \Delta_{vir}(z)\,\bar{\rho}(z)$ where $\bar{\rho}(z)$ is the cosmic average density at redshift z. It is $\Delta_{vir} = 18\pi^2$ for $\Omega_0 = 1$, whereas we take the expressions provided by Kitayama & Suto (1996) for the $\Omega_0 < 1$ cases. The center of mass of all the particles within such a sphere is then computed and used as the new center for the next iteration. The procedure is stopped, in general after few iterations, once the coordinates of the center of the sphere and its mass converge. When two clusters are found to partially overlap, the smaller one is discarded from the final list.

In Figure 1 we plot the cumulative mass function $n(>M)$, defined as the number density of objects with masses larger than M. Simulation results (histograms) are compared to the PS predictions (dashed curves) at four different redshifts, $z = 0, 0.21, 0.55, 1.40$. In each panel, the horizontal dotted line indicates the shot–noise level – the number density corresponding to finding one single cluster in all the five boxes. The vertical dotted lines indicate the mass of a halo containing 20 particles, smaller halos being not properly resolved.

As a general result, we confirm that the PS approach provides a good approximation to the N–body mass function in the region around the non–linear mass scale M_*, quite independently of the model. The ability of the PS formula to account for the different degrees of evolution in the different cases is remarkable. A similar result about the reliability of the PS formula has been also recently obtained from the analysis of Hubble–volume simulations (White 1998, private communication; see also Colberg et al. 1998). Governato et al. (1998) analysed two high–resolution simulations, for critical density and low–density CDM models, which were aimed at testing the PS formula. They found a slightly different redshift dependence of δ_c, which turns into a $\sim 6\%$ smaller value at $z \simeq 0.5$ only for the $\Omega_0 = 1$ case. Even in this case, such a difference only induces variation in σ_8 and Ω_0 which are smaller than the statistical uncertainties of our analysis (see Section 4, below).

At low masses the PS expression provides a systematic overestimate of the halo number density (see also Bryan & Norman 1998; Gross et al. 1998). However, given the flux–limit of the RDCS sample, such small masses enter only at the lowest redshifts, whereas we will mostly use the observed distributions at high–redshifts ($z \gtrsim 0.3$) to constrain our models (we will further comment in the following on the mass scales associated to RDCS clusters at different redshifts).

3.2 The mass–temperature relation

According to the spherical collapse model and under the assumption of virial equilibrium and isothermal gas distribution, the mass–temperature relation can be written as

$$k_B T = \frac{1.38}{\beta} \left(\frac{M}{10^{15} h^{-1} M_\odot} \right)^{2/3} \times \left[\Omega_0 \Delta_{vir}(z) \right]^{1/3} (1+z)\,\mathrm{keV}\,, \qquad (5)$$

where 76% of the gas is assumed to be hydrogen (see, e.g., Eke et al. 1996). The β parameter is defined as the ratio of the specific kinetic energy of the collisionless matter to the specific thermal energy of the gas,

$$\beta = \frac{\mu m_p \sigma_v^2}{k_B T}, \quad (6)$$

being $\mu = 0.59$ the mean molecular weight, m_p the proton mass and σ_v the one–dimensional cluster internal velocity dispersion. Observational data on clusters with reliable determinations of both X-ray gas temperature and galaxy velocity dispersion indicate $\beta \simeq 1$ for $T \gtrsim 3$ keV, (e.g., Lubin & Bahcall 1993; Girardi et al. 1996). The calibration of the β value using numerical simulations have been attempted by several authors (see, e.g., Bryan & Norman 1998, for a summary of numerical results), by fitting either the M–T relation of eq.(5) or the T–σ_v relation of eq.(6). Differences between the resulting β values could be due to a non–perfect virialization of the cluster or to a departure from the hydrostatic equilibrium in the ICM. Here we will refer to results based on the M–T relation, that we will use to convert masses into X-ray luminosities.

Using a Smoothed Particle Hydrodynamics (SPH) simulations of six clusters, Evrard (1991) found $\beta = 1.23$ by adopting a mass–weighted temperature definition. Evrard, Metzler & Navarro (1996) analyzed an enlarged sample of clusters, also including low–Ω_0 cases, and found an average value of $\beta = 1.05$. Their results also show some dependence on Ω_0, low–density models preferring a lower β. Bryan & Norman (1998) analyzed a set of cluster simulations based on the piecewise–parabolic–mesh (PPM) method. Using a luminosity–weighted definition for T, they found $1.27 \leq \beta \leq 1.33$. Pen (1998) used Moving–Mesh Hydrodynamic (MMH) cluster simulations for different cosmological models. By assuming an emission–weighted temperature, he found $\beta = 1.12 \pm 0.04$. Recent simulations of the Santa Barbara Cluster (Frenk et al. 1998), based on a variety of numerical techniques, converge to indicate that $\beta \simeq 1.15$. This value, which also falls within the range of previous results, will be adopted in the following as the fiducial one. We will also show results for $\beta = 1$.

3.3 The luminosity–temperature relation

The observational determination of the relation between bolometric luminosity and temperature, L_{bol}–T, at low redshift is becoming more and more accurate as larger and higher quality data sets are constructed (e.g., Mushotzky 1984; Edge & Stewart 1991; David et al. 1993). If we model the L_{bol}–T relation as

$$L_{bol} = L_6 \left(\frac{T}{6\mathrm{keV}}\right)^{\alpha} (1+z)^A \times 10^{44} h^{-2} \,\mathrm{erg\,s^{-1}}, \quad (7)$$

then low redshift data for $T \gtrsim 3\,\mathrm{keV}$ indicates $L_6 \simeq 3$ as a rather stable result, and $\alpha \simeq 2.7$–3, depending on the sample and the data analysis technique. As for the behavior at lower temperatures, Ponman et al. (1996) analysed a set of *ROSAT* observations for 22 Hickson's compact groups and found indications for a steepening of the L_{bol}–T relation below 1 keV. White, Jones & Forman (1997) analysed a set of 207 *EINSTEIN* clusters and found $\alpha \simeq 3$. Although the formal fitting uncertainties are generally small, the scatter of data points around the relation (7) is so large as to raise the question of whether it represents a good model for the observational L_{bol}–T relation. In the same paper, White et al. also confirm the result by Fabian et al. (1994) concerning the dependence of the scatter in the L_{bol}–T relation on the cooling–flow (CF) mass deposition rate, a smaller scatter being found when excluding CF clusters. Similar results about a tight L_{bol}–T relation have been obtained also by Arnaud & Evrard (1998), Markevitch (1998) and Allen & Fabian (1998) by either considering only clusters with a low CF or by correcting for the CF effect.

As for the evolution of the L_{bol}–T relation, Mushotzky & Scharf (1997) compared results from a sample of *ASCA* temperatures at $z > 0.14$ with the low–redshift sample by David et al. (1993). They found that data out to $z \simeq 0.4$ are consistent with no evolution (i.e., $A \simeq 0$), although within rather large uncertainties. Henry (1997) determined the luminosity–temperature relation for a sample of *EMSS* clusters at a median redshift $z = 0.32$ using *ASCA* temperature measurements. The decrement he found in the amplitude of the L_{bol}–T relation with respect to that by David et al. (1993) implies a marginally positive evolution with $A = 0.36 \pm 0.32$. Sadat, Blanchard & Oukbir (1998) analysed a compilation of $z > 0$ clusters taken from different authors and also found a mildly positive evolving L_{bol}–T with $0 \lesssim A \lesssim 1$.

On the theoretical side, the first attempt to describe the L_{bol}–T relation and its evolution has been developed by Kaiser (1986) for an Einstein–de Sitter (EdS) model. This model, based on the assumptions of self–similar gas evolution, can be extended to generic cosmologies and predicts $L_{bol} \propto T^2 \Delta_{vir}^{1/2}(z)$. The resulting slope of the local L_{bol}–T is definitely shallower than the observed one. On the other hand, comparisons between the self–similar scaling and results from hydrodynamical simulations have shown a general good agreement (e.g., Eke, Navarro & Frenk 1998, and references therein), especially when the effects of finite numerical resolution are taken into account (e.g., Bryan & Norman 1998). Therefore, the basic discrepancy between the predicted L_{bol}–T relation and the observed one, $L_{bol} \propto T^{\alpha}$ with $\alpha \sim 3$, must be considered as an open problem whose solution calls for additional physics, like the preheating generated by non gravitational sources (e.g., Cavaliere, Menci & Tozzi 1997; see, however, Metzler & Evrard 1997).

As for the z–dependence of the L_{bol}–T relation, Kaiser (1986) predicted an induced evolution in the XLF, for acceptable scale–free power spectra, which is opposite to the mild negative evolution found later in the data (e.g., Gioia et al. 1990). This led Kaiser (1991) and Evrard & Henry (1991) to assume that an initial entropy was imprinted in the ICM. Afterwards, this model has been generalized by

Bower (1997) to include the general redshift evolution for the minimal entropy level. As a result, a range of evolutionary patterns can be derived for L_{bol}–T and, therefore, for the XLF.

In our analysis we prefer to adopt a conservative approach and, *instead of assuming* a unique shape and evolution for the L_{bol}–T relation, we *fit* the corresponding parameters α and A to the observational data. The amplitude of the L_{bol}–T relation is taken to be $L_6 = 2.9$ which represents the best–fitting value to the data by White et al. (1997).

In order to convert bolometric luminosities into the soft *ROSAT* band $[0.5, 2.0]$ keV we need to introduce the appropriate correction. We perform it by using a Raymond–Smith code and assuming an overall ICM metallicity of 0.3 times the solar value, as actually observed. The ratio between the bolometric and the finite–band luminosity, $L_{bol}/L_{[0.5-2.0]}$, is plotted in Figure 2. In this plot we also show the differences respect to a pure bremsstrahlung spectrum with a power–law approximation for the Gaunt factor, $g(E/k_BT) \propto (E/k_BT)^{-\gamma}$. Although this simplified model for $\gamma = 0.3$ provides a reasonably accurate bolometric correction for rich clusters, it becomes inadequate for $T \lesssim 2$ keV where the effect of metal emission lines in the cluster spectra start playing a non–negligible role, increasing the emissivity above the Bremsstrahlung prediction (Sarazin 1988).

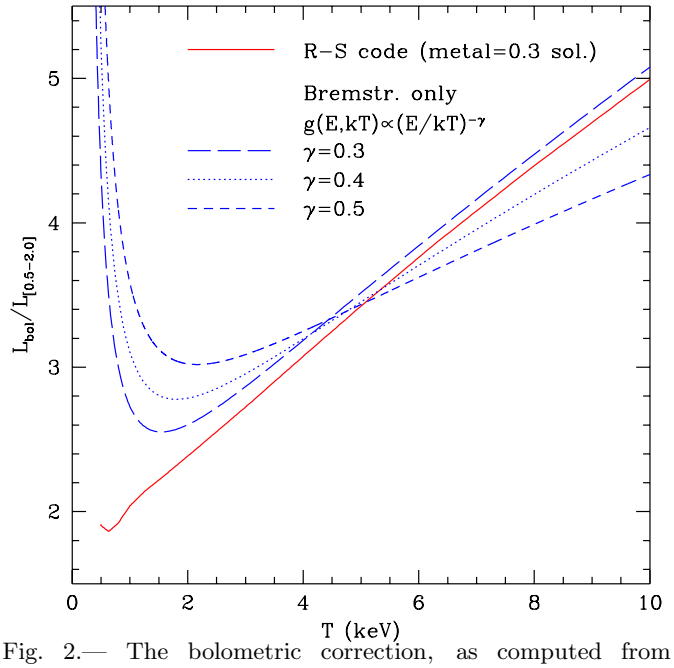

Fig. 2.— The bolometric correction, as computed from a Raymond–Smith code with ICM metallicity of $0.3 Z_\odot$ (solid curve), compared with the prediction of the pure bremssthalung for different power–law approximations for the Gaunt factor (short–dashed, dotted and long–dashed curves).

Therefore, given the above recipe to convert masses into luminosities, each model is specified by four parameters, namely $\sigma_8, \Omega_0, \alpha$ and A. The first two parameters specify the cosmological scenario, while the others are linked to the thermodynamics of the ICM. We follow a two–step procedure to place constraints on such parameters:

(a) for each value of Ω_0 we constrain Γ, or equivalently σ_8, and α with the local XLF;

(b) we use XLF at $z > 0.3$, number counts and redshift distribution from RDCS to constrain Ω_0 and A, which specify the fluctuation growth and the ICM evolution, respectively.

The amplitude of the L_{bol}–T relation is taken to be $L_6 = 2.9$ which represents the best–fitting value to the data by White et al. (1997) and it is also consistent with the data by Arnaud & Evrard (1998) for clusters without cooling flows. The remaining parameters to be determined are A, which is connected to the thermodynamics of the ICM, and Ω_0 (along with Ω_Λ), which determines the growth rate of fluctuations. The results will be presented as constraints on the Ω_0–A parameter space.

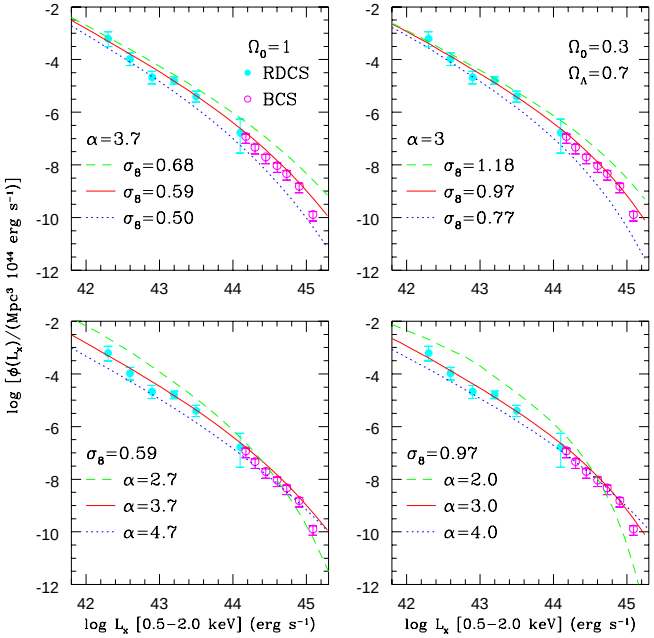

Fig. 3.— The local XLF from RCDS (filled circles) and from BCS (open circles) are compared to model predictions. Left and right panels are for an $\Omega_0 = 1$ and a flat $\Omega_0 = 0.3$ model respectively. Upper panels show the effect of changing the shape parameter Γ and, therefore, the σ_8 amplitude. Lower panels show the effect of changing the shape of the L_{bol}–T relation.

4 Results from the local XLF

The XLF in the soft *ROSAT* energy band [0.5-2.0] keV is related to the PS mass distribution according to

$$\phi(L)\, dL = \frac{dn(M)}{dM} \frac{dM}{dL}\, dL\,, \qquad (8)$$

where for simplicity L represents the luminosity in the corresponding band. In their paper, RDNG provided the XLF for the RDCS sample at different redshifts for luminosities

already converted to the local rest–frame band by applying the appropriate K–correction. We refer the reader to this paper for more details about the XLF computation.

In Figure 3 we show an example of how the XLF can be used to place constraints on the model parameter space. We plot the local XLF from the RDCS (filled circles) and the BCS at $L_X > 10^{44}\,\mathrm{erg\,s^{-1}}$ (Ebeling et al. 1997; open circles) in order to cover the bright end of the XLF, not probed by the RDCS. We also show different model predictions to emphasize the effect of changing the spectrum amplitude σ_8 (upper panels) and the shape of the L_{bol}–T relation α (lower panels) for a critical density model (left panels) and a flat low–density model with $\Omega_0 = 0.3$ (right panels). As expected, the effect of changing σ_8 in the XLF is similar to that in the mass function: a rapid change in the exponential cut–off with a smaller and smaller effect in the low–luminosity tail. A steepening of the L_{bol}–T relation (i.e., a larger α) corresponds to a larger luminosity range for a fixed temperature range. As a result, the corresponding $\phi(L)$ becomes shallower.

Constraints on the amplitude of the power spectrum (or, equivalently, the shape parameter Γ) and the slope of the local L_{bol}–T relation are placed by adopting a two–parameter χ^2–minimization procedure. The estimate of the χ^2 between model predictions and data is performed by assuming a log–normal distribution of observational uncertainties in $\phi(L)$. The probability for a model to be accepted is then computed as the probability that the data come from the parent model distribution with Gaussian random variations in logarithmic units given by the size of the error-bars. Note that the BCS and the local RDCS XLFs have two slightly different median redshifts, $\langle z \rangle \simeq 0.1$ and $\langle z \rangle \simeq 0.17$, respectively. This leads to a $\sim 6\%$ ambiguity when constraining the amplitude of the power spectrum and, therefore, σ_8.

We show in Figure 4 the results from the local XLF. For both the $\Omega_R = 0$ and $\Omega_\Lambda = 0$ cases (left and right panels, respectively) we plot the Ω_0 dependence for the shape parameter Γ, the corresponding σ_8 from the *COBE* normalization and the slope α of the L_{bol}–T relation. The shaded regions represent the 90% c.l. for model rejection. The 90% c.l. for each one of the two fitting parameters has been determined by fixing the other parameter at its best–fitting value (i.e., minimum χ^2). The dashed lines indicate the minimum–χ^2 parameters if $\beta = 1$ is assumed instead of the fiducial value $\beta = 1.15$.

As for σ_8 and Γ, we stress that these two quantities are connected by a one-to-one relation, once the power–spectrum is *COBE*–normalized. As we show in Fig. 4, they are determined with rather small uncertainties, thus confirming that the cluster abundance provides a stringent constraint on the amplitude of mass fluctuations at the cluster scale. The σ_8–Ω_0 relation plotted in Fig. 4 can be analytically fitted as:

$$\begin{aligned} \sigma_8 &= (0.58 \pm 0.02 \pm 0.04) \times \Omega_0^{-0.47+0.16\Omega_0} \quad ; \\ &\quad \Omega_\Lambda = 1 - \Omega_0 \\ \sigma_8 &= (0.58 \pm 0.02 \pm 0.04) \times \Omega_0^{-0.53+0.27\Omega_0} \quad ; \\ &\quad \Omega_\Lambda = 0 \end{aligned} \tag{9}$$

The first uncertainty corresponds to the 90% c.l. from the χ^2 minimization, whereas the second error reflects the lack of a common median redshift of the BCS and the local RDCS XLFs. Systematic uncertainties due to variations of δ_c with respect to the canonical spherical–collapse value are not included in eq.(9). However, both our analysis of N–body simulations presented and the most recent results by other authors (e.g., Governato et al. 1998; White S.D.M., private communication), converge to indicate that such uncertainties are smaller than the errors quoted in eq.(9).

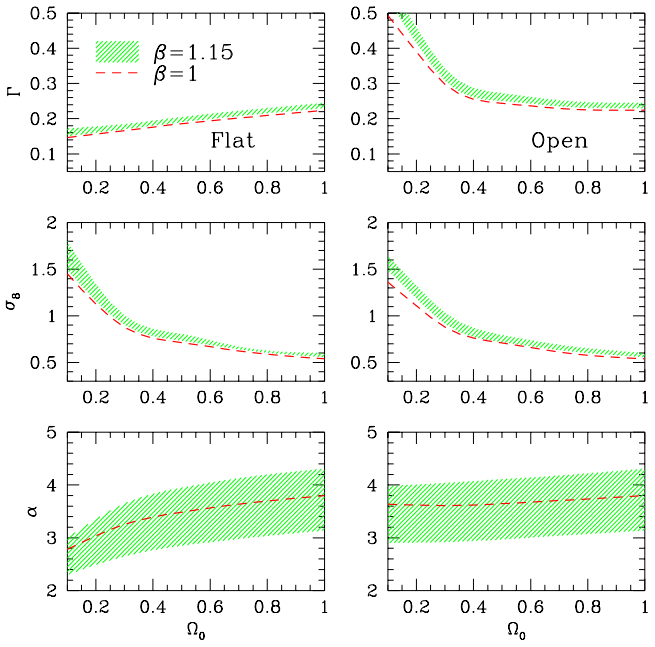

Fig. 4.— Constraints on the model parameters from the local XLF, by combining the RDCS and the high–luminosity ($L_{[0.5-2]} > 10^{44}\,\mathrm{erg\,s^{-1}}$) BCS data. Left and right panels refer to flat ($\Omega_R = 0$) and open ($\Omega_\Lambda = 0$) cases, respectively. The shaded areas indicate the 90% c.l. as deduced from the χ^2–minimization procedure, by assuming $\beta = 1.15$ (see text). The dashed curves indicates the best fitting parameters for $\beta = 1$.

The above scaling for σ_8 translates into an increasing trend for Γ if $\Omega_R = 0$ and a decreasing trend for $\Omega_\Lambda = 0$. Such a behavior is due to the different prescription for *COBE* normalization of open and flat models. For a fixed shape of the power spectrum, flat models (e.g., Bunn & White 1997) require values of σ_8 which are relatively larger and larger than those required by open models (e.g., Hu & White 1997) as Ω_0 decreases. Therefore, in order to compensate for this effects, open models select shallower spectra (i.e., larger Γs) at small Ω_0. We also note that taking $\beta = 1$ decreases the central value in eq.(9) to 0.54. This result agrees with that found by Eke et al. (1996) who in fact assumed $\beta = 1$, but used the local X-ray cluster temperature function. Furthermore, any variation of δ_c with respect to its canonical value turns into a proportional change of σ_8.

Weaker constraints are instead obtained for the shape of the L_{bol}–T relation. For open model we find $3 \lesssim \alpha \lesssim 4$, roughly independent of Ω_0, while flat models favor somewhat smaller values at low Ω_0. Such a difference is required in order to compensate for the marginally larger σ_8, for flat models at small Ω_0, corresponding to a shallower XLF. The acceptable α values cover the range of current observational determinations of the L_{bol}–T relation.

4.1 Effect of tilting the spectrum

The results so far obtained from the local XLF assume a scale–invariant primordial spectrum. On the other hand, for a fixed Ω_0, the local XLF depends to a good approximation only on σ_8. Therefore, for $n_{pr} \neq 1$, the shape parameter Γ should be varied so as to leave σ_8 unchanged. In this respect, all the constraints on A and Ω_0 that we will provide in the following are essentially independent of the assumption of a Harrison–Zeldovich primordial spectrum. In Figure 5 we show how Γ must be varied with n_{pr}, for different Ω_0, so as to keep σ_8 fixed at the best–fitting value reported in Fig. 4. For flat models we show the $\Omega_0 = 0.1, 0.3, 0.5, 1$ cases, from lower to upper curves, while $\Omega_0 = 0.2, 0.3, 0.5, 1$ cases are shown for open models, from upper to lower curves (a vanishing contribution from tensor mode fluctuations to the CMB anisotropy is always assumed). For instance, if $\Omega_0 = 1$, changing $n_{pr} = 1$ to 0.8 implies that the shape parameter must be increased from $\Gamma \simeq 0.24$ to $\simeq 0.36$ in order to provide an equally good fit to the local XLF. The shaded region indicates the 95% c.l. constraint, $\Gamma = 0.23 - 0.28(1 - 1/n_{pr})$ with 15% uncertainty, obtained by Liddle et al. (1996) from the shape of the APM galaxy power spectrum. For flat models we find that $n_{pr} \gtrsim 1$ would require $\Omega_0 \gtrsim 0.5$, while a lower density parameter implies $n_{pr} \lesssim 1$. For open models, a blue $n_{pr} > 1$ spectrum is required by $0.3 \lesssim \Omega_0 \lesssim 1$ with a rapidly increasing n_{pr} for lower Ω_0 values.

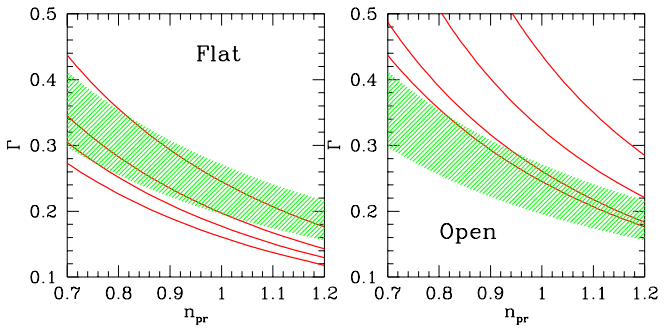

Fig. 5.— The constraints from the local XLF on the shape parameter Γ when the primordial spectral index n_{pr} takes values different from unity. Each solid curve provides the best–fitting Γs for different Ω_0. For flat models (left panel) results are provided for $\Omega_0 = 0.1, 0.3, 0.5, 1$ from lower to upper curves, while $\Omega_0 = 0.2, 0.3, 0.5, 1$ are reported for open models (right panel), from upper to lower curves. The shaded area represents the 95% c.l. constraint from the power spectrum of APM galaxies (Liddle et al. 1996).

5 Tracing the redshift evolution

In this section we will describe how the evolution of the XLF, the number counts and the redshift distribution can be used to place constraints in the (Ω_0, A) plane.

5.1 The evolution of the XLF

In Figure 6 we compare models predictions for two relevant cases with the XLF data from EMSS by Henry et al. (1992) in the redshift bin $z = [0.3 - 0.6]$ (median redshift $\langle z \rangle = 0.33$) and from the RDCS in the redshift bins $z = [0.25 - 0.50]$ and $[0.50 - 0.85]$ (median redshifts of $\langle z \rangle = 0.31$ and 0.60, respectively). The XLF for different redshift bins have been separated by $\Delta \log \phi(L) = 2$ from each other for reasons of clarity. The EMSS XLF has been converted to the 0.5–2.0 keV band as described by RDNG.

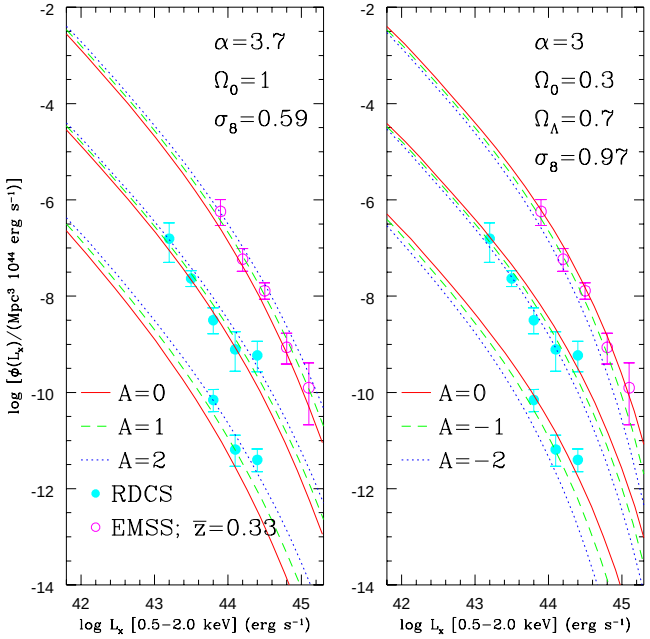

Fig. 6.— The high–redshift XLF from EMSS (open circles) and from RCDS (filled circles) are compared to model predictions. The EMSS XLF refer to the redshift interval $z = [0.3 - 0.6]$, while that from RDCS refers to $z = [0.25 - 0.50]$ and $z = [0.50 - 0.85]$ respectively. The left and the right panels are for a $\Omega_0 = 1$ and a flat $\Omega_0 = 0.3$ model, respectively. For each model and at each redshift, different curves refer to different evolutions for the L_{bol}–T relation.

In Figure 6 the shape of the power spectrum is chosen so as to fit the local XLF (cf. Fig. 4). As expected, a positive evolution of the L_{bol}–T relation, i.e. an increase of the parameter A, produces more luminous high–z objects, thus an higher XLF. The higher rate of evolution of the mass function in the $\Omega_0 = 1$ case requires a positive evolution of L_{bol}–T in order to match the lack of evolution of the XLF over a wide luminosity range. For the $\Omega_0 = 0.3$ case instead, the PS mass function evolves slowly at $z \lesssim 1$ (cf. Figure 1) so that a negligible or mild negative L_{bol}–T evolution is required by the RDCS XLF. A somewhat more negative evolution seems to be required by the

steepening of the XLF observed from the EMSS data at $L_X \gtrsim 4 \times 10^{44}\,\mathrm{erg\,s^{-1}}$, although the effect is statistically marginal.

We note that the absence of this steepening of the bright end of the XLF at high redshifts would imply a more positive evolution of the L_{bol}–T relation. For instance, we verified that assuming a non evolving XLF over the whole L_X range would require $A \simeq 2$ for an $\Omega_0 = 1$ model in Fig. 6, and $A \simeq 0.5$ for the $\Omega_0 = 0.3$ flat model.

5.2 *The number counts*

We now consider the differential cluster number counts, $n(S)$, i.e. the number of objects per steradiant with flux in the range $[S, S+dS]$. This observable can be computed starting from eq.(2) according to

$$n(S)dS \;=\; \left(\frac{c}{H_0}\right)^3 \int_0^\infty dz\, \frac{r^2(z)}{E(z)}\, n[M(S,z);z]\, \frac{dM}{dS}\, dS \tag{10}$$

(cf. Kitayama & Suto 1997) where $r(z)$ is the radial coordinate appearing in the Friedmann–Robertson–Walker metric:

$$\begin{aligned} r(z) \;&=\; \int_0^z dz\, E^{-1}(z) \qquad ; \qquad \Omega_\Lambda = 1 - \Omega_0 \\ r(z) \;&=\; \frac{2\left[\Omega_0 z + (2-\Omega_0)\left(1-\sqrt{1+\Omega_0 z}\right)\right]}{\Omega_0^2 (1+z)} \;; \\ &\quad \Omega_\Lambda = 0\,. \end{aligned} \tag{11}$$

The flux S in the *ROSAT* band is related to the luminosity according to

$$S \;=\; \frac{L}{4\pi d_L^2(z)}\,, \tag{12}$$

where $d_L(z) = r(z)(1+z)$ is the luminosity distance at redshift z. RDNG provided $n(S)$ for $S > 2 \times 10^{-14}\,\mathrm{erg\,s^{-1}cm^{-2}}$ drawn from a sample which is a factor two deeper than the one used to compute the XLF. Here we consider a further extension of the Log N–Log S to the survey flux limit. The large error bar of the faintest data point is due to incomplete optical identification at these fluxes.

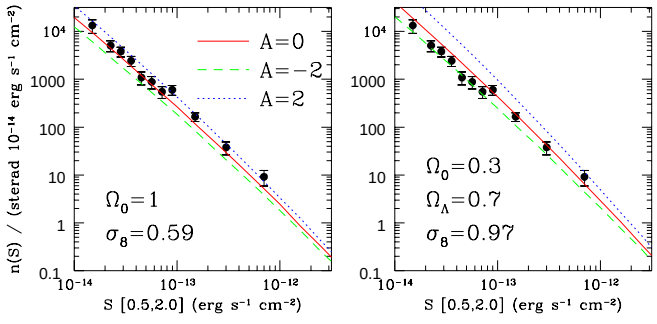

Fig. 7.— The effect of the L_{bol}–T evolution on the differential number counts, $n(S)$, for the same cosmological models shown in Figure 6.

In Figure 7 we show the effect of varying the evolution of the L_{bol}–T relation on $n(S)$ for the same models as in Fig. 6. Again, a larger value of A turns into an increase of the flux coming from clusters at a given redshift, so as to increase the number counts. Quite similar to the results from the XLF, the critical–density model favors a weak positive evolution while the low–density model requires a negative evolution for L_{bol}–T.

5.3 *The redshift distribution*

The differential redshift distribution, $n(z)$, is defined as the number of clusters above a given flux limit, in the effective survey area of the RDCS, with redshift in the range $[z, z+dz]$. Its expression is derived similarly to eq.(10) and reads

$$\begin{aligned} n(z)dz \;&=\; \left(\frac{c}{H_0}\right)^3 \frac{r^2(z)}{E(z)} \int_{S_{lim}}^\infty dS\, f_{sky}(S) \\ &\times\; n[M(S,z);z]\, \frac{dM}{dS}\, dz\,. \end{aligned} \tag{13}$$

In the above expression $S_{lim} = 4 \times 10^{-14}\,\mathrm{erg\,s^{-1}cm^{-2}}$ is the limiting flux above which the RDCS redshift distribution is complete, while $f_{sky}(S)$ is the effective flux–dependent sky–coverage appropriate for the RDCS sample (see Fig. 1 in RDNG). The upper panels of Figure 8 show the dependence of $n(z)$ on the evolution of the L_{bol}–T relation for the same two models previously considered. In this case, the high–z tail of the redshift distribution is highly sensitive to variations of the parameter A. The rather extended tail of the RDCS $dn(z)/dz$ rules out a negative A, if $\Omega_0 = 1$. On the other hand, a flat model with $\Omega_0 \simeq 0.3$ requires a mildly negative evolutionary index in order not to overproduce high–redshift clusters.

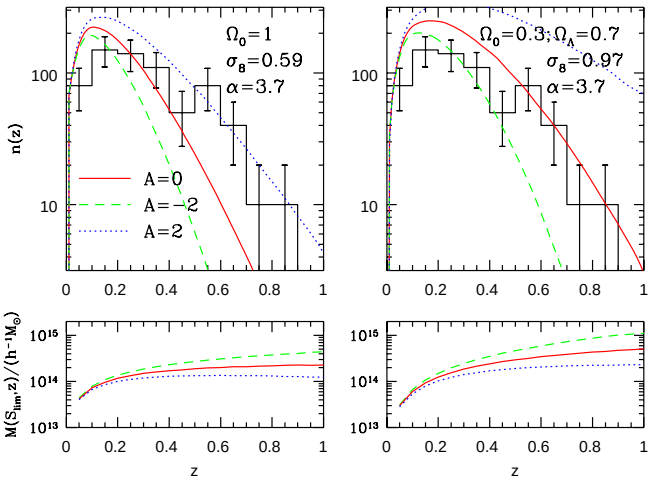

Fig. 8.— The effect of the L_{bol}–T evolution on the $n(z)$ redshift distribution, for the same cosmological models shown in Figure 6 (upper panels). The lower panels show for the same cases the mass of the smallest cluster that, at each redshift z, has a luminosity larger than $L_{lim}(z) = 4\pi d_L^2(z) S_{lim}$ (where $S_{lim} = 4 \times 10^{-14}\,\mathrm{erg\,s^{-1}cm^{-2}}$).

In the lower panels of Fig. 8 we also plot the mass corresponding to the flux limit S_{lim} as a function of the redshift for the different choices of the L_{bol}–T evolution.

This quantity corresponds to the smallest mass involved in the Press–Schechter computation of $n(z)$. Two aspects of this plot should be emphasized. Firstly, assuming a negative A, larger masses at high z are included in order to keep the flux constant; *vice versa*, for $A > 0$ the luminosity at a fixed mass increases with z and therefore, much smaller masses at high redshift are required for a cluster to emit above the RDCS flux limit. Secondly, such a minimum mass already at $z \gtrsim 0.1$ keeps values at which the Press–Schechter formula is succesfully tested against N–body simulations (cf. Fig.1). This means that the small–mass regime where the PS approach has been shown to overpredict the cluster abundance should not affect the results of our analysis.

5.4 Constraints on the A–Ω_0 plane

In order to estimate the range of A values allowed for each model we apply a one–parameter χ^2 minimization. For each Ω_0, the values of σ_8 and α are those corresponding to the best–fit to the local XLF (cf. the previous section). A global summary of the resulting constraints on the Ω_0–A plane from the three observational constraints is shown in Figure 9. For both flat (left panels) and open (right panels) models, the shaded areas correspond to the 90% c.l. for A. As a general result, these findings confirm on a more quantitative ground that $\Omega_0 \simeq 1$ models prefer a positive L_{bol}–T evolution, while lower A values are required by smaller Ω_0.

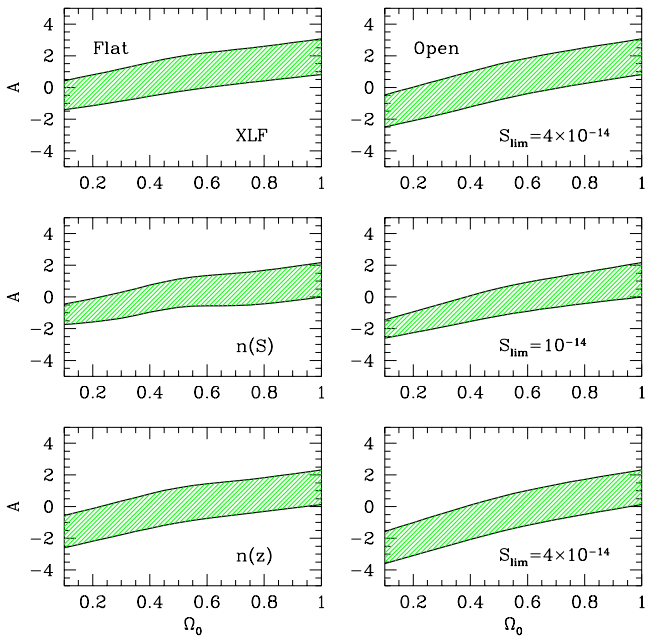

Fig. 9.— Constraints at the 90% c.l. on the Ω_0–A plane from the $z > 0.3$ XLF, number counts $n(S)$ and redshift distribution $n(z)$ (from upper to lower panels, for both flat and open models (left and right panels respectively). The limiting fluxes of the samples (in units of $\mathrm{erg\,s^{-1}cm^{-2}}$) from which the XLF, $n(S)$ and $n(z)$ are derived are also indicated.

As expected, the constraints provided by XLF, $n(S)$ and $n(z)$ are almost coincident, although the XLF tends to prefer marginally larger values of A. Small differences between such constraints may be expected in principle. Indeed, they come from somewhat different samples. The XLF constraint includes the EMSS results for $L_{[0.5,2]}$ at $\langle z \rangle = 0.33$, as well as the RDCS data above $S_{lim} = 4 \times 10^{-14}\,\mathrm{erg\,s^{-1}cm^{-2}}$. The $n(S)$, instead, has been computed for RDCS clusters down to $S_{lim} = 1 \times 10^{-14}\,\mathrm{erg\,s^{-1}cm^{-2}}$, while $n(z)$ is based on the same flux–limit as the XLF.

A tentative analytic fit of the constraints on the Ω_0–A plane from the redshift distribution is provided by the expressions

$$A = (3\Omega_0 - 2) \pm 1 \quad ; \quad \Omega_R = 0\,;$$
$$A = (4\Omega_0 - 3) \pm 1 \quad ; \quad \Omega_\Lambda = 0\,. \qquad (14)$$

A similar result has recently been obtained, only for the open models, by Sadat et al. (1998) using the redshift distribution of the EMSS sample. As a general result, it is evident how an independent determination of the evolution of the L_{bol}–T relation and a deeper understanding of the nature of its scatter can turn into a constraint on the density parameter. For instance, if a redshift–independent L_{bol}–T relation is assumed (i.e. $A = 0$), then the evolution of the XLF implies $\Omega_0 = 0.4^{+0.3}_{-0.2}$ if $\Omega_\Lambda = 0$ and $\Omega_0 \leq 0.6$ if $\Omega_R = 0$. These findings are consistent with those obtained by Eke et al. (1998) from the analysis of the X–ray temperature function at $z \lesssim 0.4$, also based on a non–evolving L_{bol}–T relation.

As for the physical meaning of the evolution parameter A, detailed models involving both the gravitational shock heating and non–gravitational heating (see Cavaliere, Menci & Tozzi 1997, Tozzi & Norman in prep.), predict a range of A values between 0 and 1.5 at the cluster mass scale, and slightly lower values, $-0.5 \lesssim A \lesssim 1$, for groups. This result holds if the non–gravitational heating rate has a smooth dependence on the redshift, as suggested by the average star formation rate derived from deep galaxy surveys (e.g., Madau et al. 1996). However, the duration and the epoch of the heating of the ICM, which is not well known at present, critically affects the effective value of A, so that a self consistent modeling of the feedback processes from galaxies is needed in order to constrain A within a narrow range. This justifies our present choice to leave A as a parameter free to be fit by the evolution of the XLF.

6 Conclusions

In this paper we have used observational results from the Rosat Deep Cluster Survey by Rosati et al. (1998) to place constraints on cosmological models. The unprecedented extension of the RDCS both in redshift ($z \lesssim 0.8$) and fluxes ($S \gtrsim 1 \times 10^{-14}\,\mathrm{erg\,s^{-1}cm^{-2}}$ in the [0.5-2.0] keV band) makes it, in principle, a suitable baseline over which the evolutionary pattern of the cluster abundance and, therefore, the density parameter Ω_0, can be investigated. A necessary ingredient for this analysis is the physics of the intra–cluster gas, which drives the relation between the

distribution of cluster halo masses and the observed distribution of X–ray luminosities. To this purpose, we adopt a parametrical approach in which the shape of the local L_{bol}–T relation, its evolution and the parameters specifying the cosmological models are *all* fitted against observational data.

Firstly, we have used the local XLF from RDCS and the extension at high luminosities from the XLF of the Brightest Cluster Sample (Ebeling et al. 1997) to fix the r.m.s. fluctuation amplitude at the cluster mass scale and the shape of the local L_{bol}–T relation. Secondly, we have used the evolving XLF, the flux number counts and the redshift distribution with the aim of constraining the density parameter Ω_0 and the evolution of the L_{bol}–T relation.

The main results of our analysis can be summarized as follows.

(a) A careful comparison between the PS predictions and N–body simulations confirms that this analytical approach for the distribution of virial halo masses is adequate over a rather large mass range around the non–linear mass scale. The low mass tail, where the PS formula overpredicts the halo abundance, has been shown to lie outside the mass range probed by RDCS clusters.

(b) The local XLF data constrain the amplitude of the power spectrum according to

$$\begin{aligned} \sigma_8 &= (0.58 \pm 0.06) \times \Omega_0^{-0.47+0.16\Omega_0} \quad ; \\ &\quad \Omega_\Lambda = 1 - \Omega_0 \\ \sigma_8 &= (0.58 \pm 0.06) \times \Omega_0^{-0.53+0.27\Omega_0} \quad ; \\ &\quad \Omega_\Lambda = 0\,. \end{aligned} \tag{15}$$

This result agrees with analyses of the X–ray temperature function (e.g., Viana & Liddle 1996; Eke et al. 1996; Markevitch 1998), the optical virial mass function (e.g., Girardi et al. 1998) and the X–ray cluster number counts alone.

As for the shape of the local L_{bol}–T relation, we find $3 \lesssim \alpha \lesssim 4$, quite independent of the cosmological model and in general agreement with observational results (e.g., David et al. 1993; White et al. 1997).

(c) From the observed evolution of the XLF we constrain the density parameter Ω_0 and the evolution parameter A of the L_{bol}–T relation. We find that $\Omega_0 = 1$ models require a positive evolution of the L_{bol}–T relation with $1 \lesssim A \lesssim 3$. A non–evolving L_{bol}–T ($A = 0$), consistent with data at $z \lesssim 0.4$ (Mushotzky & Scharf 1997), implies $\Omega_0 = 0.4^{+0.3}_{-0.2}$ for open models and $\Omega_0 \lesssim 0.6$ for flat models.

This paper set out to address the two principal issues given in the Introduction. In summary, the above results lead us to conclude that: (1) Available data on the local cluster XLF place robust constraints on σ_8 as a function of Ω_0 [cf. eqs.(9)], without any *a priori* assumption about the local L_{bol}–T relation and; (2) Present uncertainties in the evolution of the L_{bol}–T relation do not as yet give strong constraints on Ω_0, even with a high–redshift sample as deep as RDCS.

Samples like RDCS will represent a fundamental basis for the study of distant clusters in the years to come. The next generation of X–ray satellites and the already available large optical telescopes should open the possibility of determining cluster masses via X–ray temperature measurements, virial analysis and gravitational lensing studies. Carrying on such observations for an even limited number of clusters, extracted from a well defined statistical sample, will determine both the evolution of the cluster internal dynamics and the value of the cosmological density parameter.

S.B. wishes to acknowledge the European Southern Observatory and the Johns Hopkins University for hospitality during several phases of preparation of this work. We wish to thank Hugh Couchman for the generous sharing of his adaptive P3M code. We are also grateful to Alfonso Cavaliere and Riccardo Giacconi for stimulating discussions and continuous encouragement on this work, and to Pat Henry for a careful reading of the paper. P.R. thanks the Telescope Allocation Committees of Kitt Peak National Observatory, Cerro Tololo Inter-American Observatory, and ESO for the allocation of generous observing time. This work has been supported by NASA grants NAG 8-1133 and NAG 5-3537.

REFERENCES

Allen, S.W., & Fabian, A.C., 1998, MNRAS. 297, 63
Arnaud, K.A., & Evrard, A.E., 1998, MNRAS, submitted, preprint astro–ph/9806353
Bahcall, N.A., & Cen, R., 1992, ApJ, 407, L49
Bardeen, J.M., Bond J.R., Kaiser N., & Szalay, A.S., 1986, ApJ, 304, 15
Bartlett, J.G., & Silk, J., 1993, ApJ, 407, L45
Baugh, C.M., & Efstathiou, G., 1993, MNRAS, 265, 145
Bower, R.G., 1997, MNRAS, 288, 355
Bryan, G.L., & Norman M.L., 1998, ApJ, 495, 80
Bunn, E.F., & White M., 1997, ApJ, 480, 6
Burke, D.J., Collins, C.A., Sharples, R.M, Romer, A.K., Holden, B.P., & Nichol, R.C., 1997, ApJ, 488, 83
Carlberg, R.G., Yee, H.K.C., Ellingson, E., Abraham, R., Gravel, P., Morris, S.M., & Pritchet, C.J., 1996, ApJ, 462, 32
Carlberg, R.G., Morris, S.L., Yee, H.K.C., & Ellingson, E., 1997, ApJ, 479, L19
Castander, F.J., 1995, Nature, 377, 39
Cavaliere, A., Menci N., & Tozzi P., 1997, ApJ, 484, L21
Cavaliere, A., Menci N., & Tozzi P., 1998, ApJ, 501, 493
Colafrancesco, S., & Vittorio, N., 1994, ApJ, 433, 443
Colberg, J.M., et al., 1998, in proceedings of The 14th IAP Colloquium: Wide Field Surveys in Cosmology (Paris, 1998 May 26-30), eds. S.Colombi, Y.Mellier, p.247
Collins, C.A., Burke, D.J., Romer, A.K., Sharples, R.M., & Nichol, R.C., 1997, ApJ, 479, L11
Couchman, H.M.P., 1991, ApJ, 368, L23
David, L.P., Slyz, A., Jones, C., Forman, W., Vrtilek, S.D., & Arnaud K.A., 1993, ApJ, 412, 479

Ebeling, H., Edge, A.C., Fabian, A.C., Allen, S.W., Crawford, C.S., & Böhringer, H., 1997, ApJ, 479, L101
Edge, A.C., & Stewart, G., 1991, MNRAS, 252, 414
Eke, V.R., Cole, S., & Frenk, C.S., 1996, MNRAS, 282, 263
Eke, V.R., Navarro, J.L., & Frenk, C.S., 1998, ApJ, 503, 569
Eke, V.R., Cole, S., Frenk, C.S., & Henry, J.P., 1998, MNRAS, 298, 114
Evrard, A.E., 1991, in Clusters of Galaxies, ed. M.Fitchett & W.Oegerle (Cambridge: Cambridge University Press)
Evrard, A.E., & Henry, J.P., 1991, ApJ, 383, 95
Evrard, A.E., Metzler, C.A., & Navarro, J.F., 1996, ApJ, 469, 494
Fabian, A.C., Crawford, C.S., Edge, A.C., & Mushotzky, R.F., 1994, MNRAS, 267, 779
Fan, X., Bahcall, N.A., & Cen R., 1997, ApJ, 490, L123
Frenk, C.S., White, S.D.M., Efstathiou, G., & Davis M., 1990, ApJ, 351, 10
Frenk, C.S., et al., 1998, preprint
Gioia, I.M., Henry, J.P., Maccacaro, T., Morris, S.L., Stocke, J.T., & Wolter, A., 1990, ApJ, 356, L35
Girardi, M., Fadda, D., Mardirossian, F., Mezzetti, M., & Biviano, A., 1996, ApJ, 457, 61
Girardi, M., Borgani, S., Giuricin, G., Mardirossian, F., & Mezzetti, M., 1998, ApJ, 506, 45
Górski, K.M., Banday, A.J., Bennett, C.L., Hinshaw, G., Kogut, A., Smoot, G.F., & Wright, E.L., 1996, ApJ, 464, L11
Governato, F., Babul, A., Quinn, T., Tozzi, P., Baugh, C.M., Katz, N., & Lake G., 1998, MNRAS, submitted
Gross, M.A.K., Somerville, R.S., Primack, J.R., Borgani, S., & Girardi, M., 1998, in Proceedings of the 12^{th} Potsdam Cosmology Workshop "Large–Scale Structure: Tracks and Traces, p.171
Henry, J.P., Gioia, I.M., Maccacaro, T., Morris, S.L., Stocke, J.T., & Wolter A., 1992, ApJ, 386, 408
Henry, J.P., 1997, ApJ, 489, L1
Hu, W., & White, M., 1997, ApJ, 486, L1
Kaiser, N., 1984, ApJ, 284, L9
Kaiser, N., 1986, MNRAS, 222, 323
Kaiser, N., 1991, ApJ, 383, 104
Kitayama, T., & Suto, Y., 1996, ApJ, 469, 480
Kitayama, T., & Suto Y., 1997, ApJ, 490, 557
Lacey, C.G., & Cole, S., 1994, MNRAS, 271, 676
Liddle, A.R., Lyth, D.H., Schaefer, R.H., Shafi, Q., & Viana, P.T.P., 1996, MNRAS, 281, 531
Lilje, P.B., 1992, ApJ, 386, L33
Lubin, L.M., & Bahcall, N.A., 1993, ApJ, 415, L17
Madau, P., Ferguson, H.C., Dickinson, M.E., Giavalisco, M., Steidel, C.G., & Fruchter, A., 1996, MNRAS, 283, 1388
Markevitch, M., 1998, ApJ, 504, 27
Mathiesen, B., & Evrard, A.G., 1998, MNRAS, 295, 769
Metzler, C., & Evrard, A.E., 1997, preprint astro–ph/9710324
Mushotzky, R.F., 1984, Phys. Scripta, T7, 157
Mushotzky, R.F., & Scharf, C.A., 1997, ApJ, 482, L13
Oukbir, J., & Blanchard, A., 1992, A&A, 252, L21
Peebles, P.J.E., 1993, Physical Cosmology (Princeton: Princeton University Press
Pen, U.L., 1998, ApJ, 498, 60
Ponman, T.J., Bourner, P.D.J., Ebeling, H., & Böhringer H., 1996, MNRAS 283, 690
Press, W.H., & Schechter, P., 1974, ApJ, 187, 425 (PS)
Primack, J.R., in Critical Dialogues in Cosmology, ed. Neil Turok (Teaneck, NJ: World Scientific).
Reichart, D.E., Nichol, R.C., Castander, F.J., Burke, D.J., Romer, A.K., Holden, B.P., Collins, C.A., & Ulmer, M.P., 1998, ApJ, submitted, preprint astro–ph/9802153
Rosati, P., Della Ceca, R., Burg, R., Norman, C., & Giacconi, R., 1995, ApJ, 445, L11
Rosati, P., Della Ceca, R., Norman, C., & Giacconi, R., 1998, ApJ, 492, L21(RDNG)
Sadat, R., Blanchard, A., & Oukbir, J., 1998, A&A, 329, 21
Sarazin, C.L., 1988, X–ray Emission from Clusters of Galaxies (Cambridge: Cambridge University Press)
Scharf, C.A., Jones, L.R.L., Ebeling, H., Perlman, E., Malkam, M., & Wegner G. 1997, ApJ, 477, 79
Viana, P.T.P., & Liddle, A.W., 1996, MNRAS, 281, 323
Viana, P.T.P., & Liddle, A.W., 1998, MNRAS, in press, preprint astro–ph/9803244
Vikhlinin, A., McMamara, B.R., Forman, W., Jones, C., Quintana, H., & Hornstrup, A., 1998, ApJ, 502, 558
White, D.A., Jones, C., & Forman, W., 1997, MNRAS, 292, 419
White, M., Gelmini, G., & Silk, J., 1995, Phys. Rev. D, 51, 2669
White, S.D.M., Efstathiou, G., & Frenk, C.S., 1993, MNRAS, 262, 1023